Microfluidics and Nanofluidics (2023) 27:16
https://doi.org/10.1007/s10404-022-02620-5

RESEARCH PAPER

Enhanced particle focusing and sorting by multiple sheath stream in contraction–expansion microchannel

Zhibin Wang[1,2] · Tieshan Zhen[1,2] · Fan Wu[1,2] · Songping Mo[1,2] · Lisi Jia[1,2] · Ying Chen[1,2]

Received: 6 October 2022 / Accepted: 31 December 2022 / Published online: 18 January 2023

Abstract

Microfluidic devices have great potential in cell analysis, and cell focusing/sorting is one of the basic manipulation processes required for cell analysis. This paper proposes a microchannel with a contraction–expansion structure to improve the focusing and sorting performances of particles, integrating multiple sheath fluid inputs from a single inlet. To prove its applicability, the influences of the main structural parameters on the performance were studied using a fluid–particle interaction model. The focusing and sorting performances improved by 31.9% and 55.2%, respectively, when the sheath streams increased from one to two due to the strengthening Dean vortex. Optimization of each parameter significantly improved the performance, and the improvement exceeded 40%. The forces on the particles in this contraction–expansion microchannel with multiple sheath liquid flows were analyzed. A fitting correlation between the particle diameter and the minimum channel length required to achieve complete focusing was obtained, and the formula's accuracy was verified. This result is expected to be significant for selecting and optimizing contraction–expansion-type microchannels with sheath flows.

Keywords Microfluidics · Multiple sheath fluid streams · Contraction–expansion structure · Fluid–particle interaction · Particle focusing

1 Introduction

Microfluidic device technology (Su et al. 2020), a transformative technology, was proposed by (Manz et al. 1990) and has since been significantly developed. Its development has brought tremendous changes to clinical testing technology, making it possible to miniaturize clinical testing instruments (Kalyan et al. 2021; Soares et al. 2019; Wang et al. 2018). The focusing and sorting of microparticles/cells based on microfluidic technology have broad application prospects in the fields of medical research and development (Carlo et al. 2009; Seo et al. 2012), biochemical testing (Berger et al. 1983; Magnin 2009), and quality monitoring (Sun et al. 2013; Xiang et al. 2015). For example, inertial focusing and sorting in microfluidics can achieve rapid particle/cell focusing and sorting with low sample consumption (Jiang et al. 2021; Zhou et al. 2021). After this, a variety of physical and chemical characteristics of individual cells (Stavrakis et al. 2019) can be easily measured for a range of applications, including the diagnosis of blood cancers (Hasegawa et al. 2013), T cell phenotyping (De Rosa et al. 2001), and the detection of rare cells (Gross et al. 1993).

There are two ways to achieve particle focusing and sorting in microfluidics: active and passive manipulation. Passive approaches have the advantages of being simple and less prone to damage because they rely only on the channel geometry and inherent hydrodynamic forces for functionality. Among the passive approaches, the inertial microfluidics approach, which takes advantage of the size-dependent hydrodynamic effects in microchannels, has become a promising approach for particle and cell focusing and sorting due to its high-volume and high-throughput sample processing. Inertial focusing was first discovered in a circular tube by Segre and Silberberg (Segre and Silberg 1961). Since then, many studies have applied inertial particle migration to microfluidic chips (Hur et al. 2010). For example, Bhagat et al. (2008) studied the focusing characteristics of particles in a rectangular linear microchannel. They found that the focus position of

✉ Ying Chen
chenying@gdut.edu.cn

[1] School of Material and Energy, Guangdong University of Technology, Guangzhou 510006, Guangdong, China

[2] Guangdong Provincial Key Laboratory of Functional Soft Matter, Guangzhou 510006, Guangdong, China

the particles was closely related to the aspect ratio of the microchannel. Subsequently, microchannel structures have evolved from the early straight channels to channels with various designs, such as variable cross sections and curves (Huang et al. 2020; Tang et al. 2020). Further developing highly efficient particle-focusing/sorting microchannels remains a popular research topic (Kalyan et al. 2021).

Among the developed structures, the contraction–expansion structure has recently been attracting attention because it can induce Dean flow in the fluid to improve the focusing and sorting effect (Shahraki et al. 2022; Jiang et al. 2019, 2021). For this reason, Choi et al. (2008) used a straight flow channel to establish a concave–convex structure to achieve symmetric cell focusing. However, due to the symmetric flow channel structure, there were two focus positions for the cells (Raihan et al. 2022). Recently, Li et al. (2016) fabricated a three-dimensional concave–convex structure on the top wall of a microchannel to focus Euglena. Fan et al. developed and optimized microchannels for focusing particles with triangular sharp-angle concave–convex structures (Fan et al. 2014) and optimized them (Fan et al. 2018). The particles were concentrated in a single stream through a combination of inertial forces and vortices. Moreover, sheath flow was also used to improve the focusing/sorting performance. Lee et al. (2014) used a horizontal contraction–expansion flow channel combined with a sheath fluid to achieve particle focusing. However, only a single stream of sheath flow was used in the contraction–expansion microchannel. The influence mechanisms of the sheath parameters and whether the focusing and sorting effects of particles can be improved without increasing the sheath flow from a single inlet remain to be determined. Furthermore, the channel length required for particle focusing in the contraction–expansion channel must be determined.

This paper proposes an asymmetric contraction–expansion array microchannel with the introduction of multiple sheath fluid streams to focus and sort particles. We propose to improve the focusing and sorting performances of particles through the coordination of multiple sheath streams. To prove the superior performance of the proposed microchannel, the influencing mechanism of the main structural parameters was studied using a particle dynamics model considering the fluid–particle interactions. The focusing and sorting performances improved by 31.9% and 55.2%, respectively, when the sheath streams increased from one to two due to the strengthening Dean vortex. The optimization of each parameter significantly improved the channel performance, and the improvement exceeded 40%. Moreover, we analyzed the force mechanism of the particles in the proposed microchannels and obtained an expression for the lateral forces on the particles. According to the lateral force analysis, an equation for the minimum length required for the particles to be entirely focused was obtained by fitting, and the accuracy of the equation was verified.

2 Models and methods

2.1 Physical model

This paper proposes a contraction–expansion array structure microchannel to introduce multiple sheath fluid streams simultaneously to achieve particle focusing and sorting. The microchannel structure is shown in Fig. 1. The total length was 7.5 mm, and the height of the entire microchannel was 40 μm. The channel width in the constricted area of the channel was 100 μm, and the length was 600 μm. The width of the expanded area was 450 μm, and the length was 700 μm. The inlet velocities of the sample and sheath fluid were 0.095 and 0.475 m/s, respectively. These values were selected according to the optimal results of Lee et al. (2011). The angle between the sample and sheath fluid inlets was set to α. For multiple sheath inlets, the first sheath inlet was fixed, and the distance between the first and second sheath liquid inlets was defined as inlet position x_{in}. The adjacent inlet distance was set to 1300 μm for subsequent inlets. The sheath liquid inlet width was defined as β.

2.2 Boundary conditions and numerical solution method

Since the particles involved in this study were small, the gravitational forces were negligible compared to the surface forces. In addition, the interactions between the particles were ignored due to the low particle concentration. The fluid flow was treated as laminar due to the low Reynolds numbers. To simplify the analysis, the solid particles dispersed in the deionized water solution were uniformly spherical. The Lagrangian model was used to simulate the dynamic behaviors of the particles, and the positions and velocities of the particles, which changed with time, were obtained. The detailed calculation method is shown in the Supplementary Information. The relevant boundary conditions of the numerical calculation are shown in Table 1.

2.3 Model and grid independence verification

To verify the rationality of the model, the above-mentioned numerical simulation method and solution strategy were used to numerically simulate the particle-focusing structure proposed by Lee et al. (2011), and the results were compared with experimental results. In the experiments of Lee et al. (2011), the particles migrated in the contraction–expansion microchannel with sheath flow, as shown in Fig. 2a. The processes of the particles and fluid were the same as those

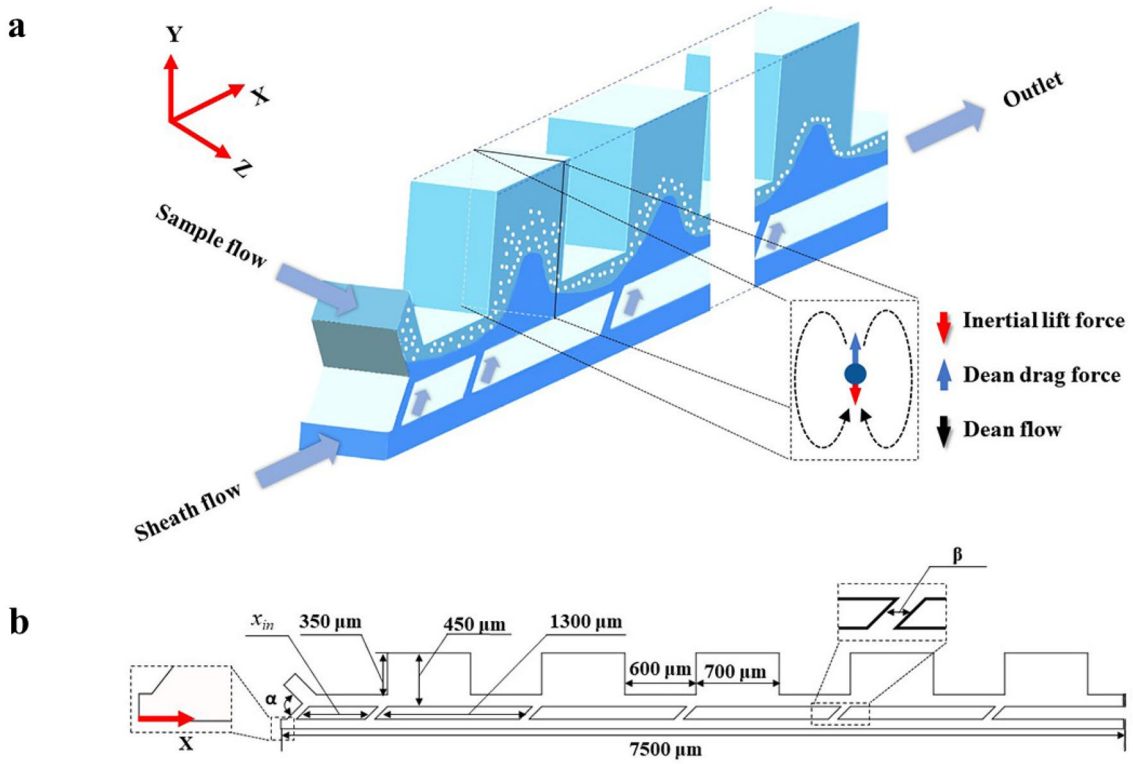

Fig. 1 Schematic diagram of multiple sheath fluid contraction–expansion microchannels: **a** perspective view and **b** two-dimensional view

Table 1 Boundary conditions

Boundary conditions	Content description
Wall	No slip
Sample inlet	0.095 m/s
Sheath fluid inlet	0.475 m/s
Outlet	Pressure outlet

in our microchannel. The physical parameters and conditions used in the model were all consistent with the experiments. The qualitative and quantitative comparisons are shown in Fig. 2b, c, respectively. The comparisons showed that the simulation results were very similar to the experimental results, and the average particle focus position deviation was 4.43%. Therefore, the numerical model in this paper can be considered reasonable and credible.

To determine the appropriate computational grid size, grid independence verification was performed. Three different grids were used to divide the simulation area. The grid independence verification results are shown in Table 2. By comparing the focus positions of the particles, it was found that although the grid with 1,209,043 elements contained 2.45 times as many elements as the grid with 492,758 elements, the difference between their calculation results was only 0.31%. Therefore, based on the calculation cost, a model with 492,758 grid elements was selected for subsequent calculations.

3 Results and analysis

3.1 Enhanced focusing and sorting by multiple sheath fluid

In this section, we study the mechanism through which the fluid flow in the multiple sheath fluid contraction–expansion array microchannels affects the focusing/sorting behavior of particles and analyze the flow field and particle dynamics. The impacts of the entrance angle, position, width, and number were analyzed, and the optimal results obtained in a previous study were used in the subsequent analysis. Since the processing and manufacturing of a microchannel outlet on the y-axis are easier in practical applications, our flow channel design focused on the particle-focusing effect along the y-axis. To quantify the performances, the standard deviation σ of the particle-focusing position and the particle separation resolution R were introduced to evaluate the focusing and sorting performances, respectively. The definitions are shown in the Supplementary Information.

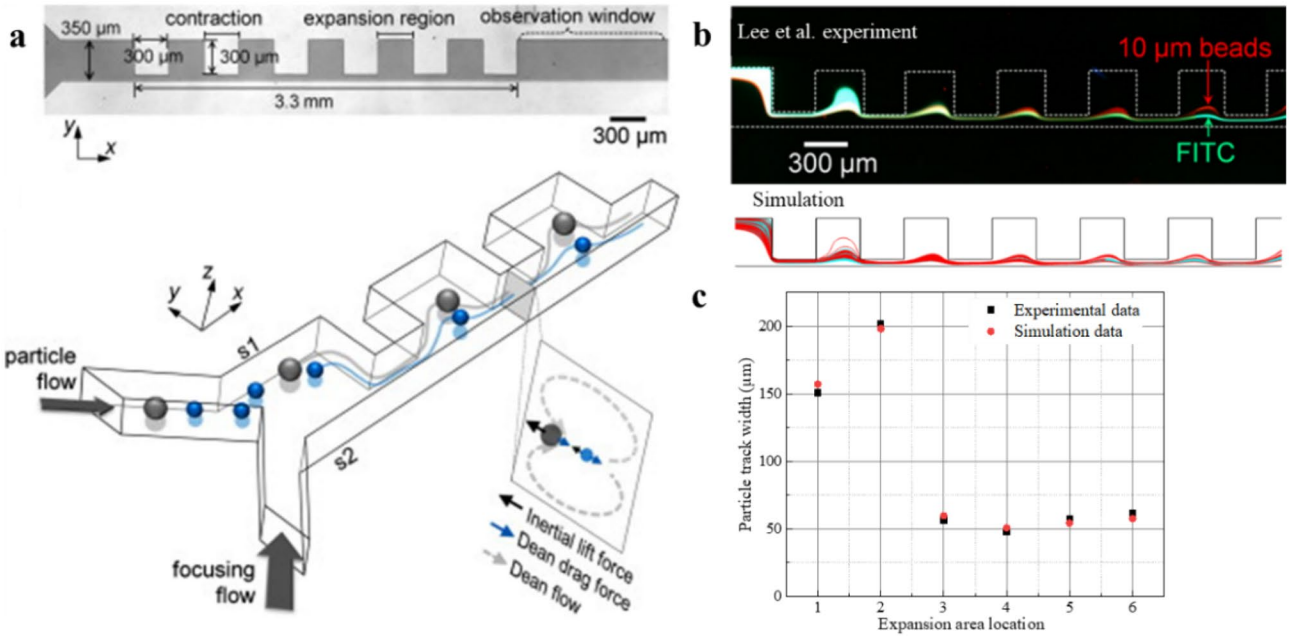

Fig. 2 **a** Channel structure and physical process in experiments of Lee et al. **b** Qualitative comparison of numerical simulation and experimental results. **c** Quantitative comparison of numerical simulation and experimental results

Table 2 Grid independence verification

Number of grid elements	Average particle-focusing position on *y*-axis (μm)	Deviation
254,670	40.7350	1.06%
492,758	40.7369	0.31%
1,209,043	40.7385	/

3.1.1 Effect of different sheath fluid inlet angles on particle focusing

In the analysis presented in this sub-section, the number of sheath liquid inlets was set to six, $x_{in} = 890$ μm, and $\beta = 100$ μm. To compare the effects of various sheath fluid inlet angles α on the particle focusing, the flow field of the microchannel was first analyzed. As the fluid flowed from the expanding region to the contracting area, centrifugal action pushed the sample flow to the outside. It triggered Dean flow, intensifying particle migration along the *y*-axis and accelerating the particle focusing. Figure 3a shows the Dean velocity values in different contraction regions for channels with different angles α. When $\alpha = 90°$, the Dean velocity of the channel cross section was larger than those at other angles, which would generate stronger Dean vortices. Since the Dean vortex was more robust, the particles were more likely to migrate laterally in the flow channel to achieve focus faster.

The flow field will inevitably affect the dynamic behavior of the particles. Therefore, we further analyzed the focusing behavior of the particles in the structure with different sheath fluid introduction angles. Figure 3b shows the locations of the 15-μm particles in the exit cross section for five different α values. The error bars represent the standard deviation σ of the particle-focusing position to indicate the focusing performance. In this study, the particle positions in the sample liquid inlet of the microchannel were randomly distributed. When α was 90°, the focusing effect of the particles was the best of all the angles. The standard deviation σ decreased by 63.1% compared to that when $\alpha = 30°$. This was because the sheath flow had a weak clamping effect when the angle was too small. While the sheath had a strong impact on the particles when the angle was too large, which was not conducive to the regular arrangement of particles.

3.1.2 Influence of position of sheath liquid inlet on focusing and sorting of particles

Due to the different sheath fluid inlet positions, the forces on the particles of the flow channel will be different. Therefore, we analyzed the effect of the sheath liquid inlet position x_{in} on the particle motion in the microchannel. The angle α was set to the optimal value of 90°. The number and width of the sheath liquid inlets were kept at six and 100 μm, respectively. The four channel structure devices were simulated, and the particle distribution of the exit cross section is

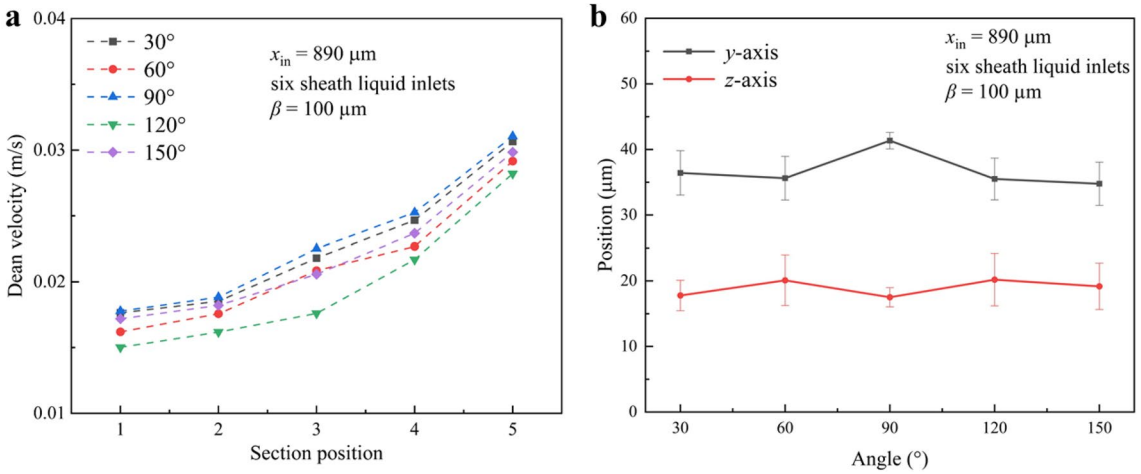

Fig. 3 Impact of inlet angles (α): **a** Dean velocity in the middle section of each contraction–expansion structure, **b** distribution of the particle focus positions at the exit

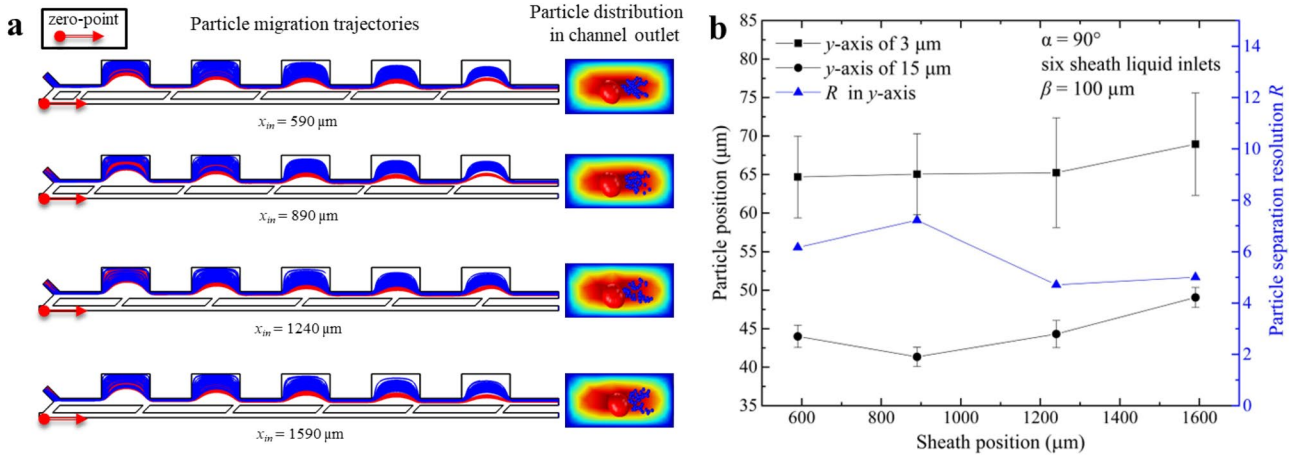

Fig. 4 Effects of the sheath inlet positions: **a** particle migration trajectories (left) and particle distributions at the channel outlet (right), **b** focus positions of particles at the channel outlet

shown in Fig. 4a. The focusing and sorting performances of the particles in the exit cross sections of these four channels are shown in Fig. 4b.

After the perturbation of the Dean vortex in the five expansion regions, the four channels all had excellent focusing effects on the particles. The focusing along the *y*-axis was best when the sheath inlet position was $x_{in} = 890$ μm. The focusing performance maximum increased by 40.8% compared to that of the sheath inlet position of $x_{in} = 1240$ μm. This was because the inflow of the sheath fluid in the expansion area was more conducive to the intensification of the Dean flow. The separation resolution R should be as large as possible for particles of both sizes to achieve particle sorting. For the 15-and 3-μm particles along the *y*-axis, the separation resolution R was the maximum for the sheath fluid inlet position of $x_{in} = 890$ μm. Therefore, the channel with the sheath fluid inlet position of $x_{in} = 890$ μm exhibited a better particle sorting performance than the channels with the sheath fluid inlet positions of $x_{in} = 1240$, 1590, and 540 μm. The sorting performance with $x_{in} = 890$ μm improved by 53.3% compared to that with $x_{in} = 1240$ μm. This was because the Dean flow enhanced the separation effect of particles of different sizes.

3.1.3 Effect of sheath liquid inlet width on particle-focusing and sorting

In the simulations discussed in this sub-section, the angle α was set to 90°, and the sheath inlet position was set to $x_{in} = 890$ μm based on the optimal result. The number of sheath liquid inlets was kept at six. Figure 5 shows the effect of the sheath inlet width on the particle focusing and sorting,

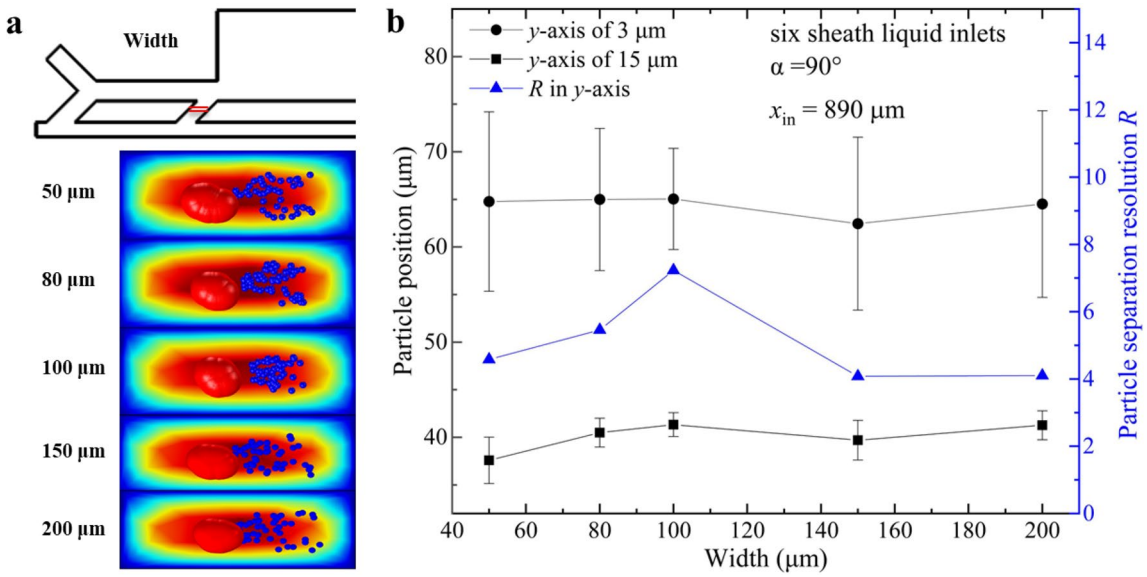

Fig. 5 Effects of sheath inlet widths: **a** particle distribution at the outlet, **b** focus positions of particles at the channel outlet

and all five channels exhibited excellent focusing performances. Along the *y*-axis, the best focusing performance was achieved for the 15-and 3-μm particles when the channel sheath inlet width was 100 μm. σ was reduced by 45.6% when the width increased from 50 to 100 μm, which indicates that the focusing performance was greatly increased. The fluid velocity decreased with increasing sheath inlet width because of the constant flow rate of the sheath flow. In particular, the extrusion forces on the particles became weak when the sheath inlet was widened. As a result, the sheath flow had a weak clamping effect for a large sheath inlet width. The sheath had a strong impact on the particles when the width was too narrow, which was not conducive to the regular arrangement of particles. For the 15- and 3-μm particles along the *y*-axis, the channel separation resolution *R* was the greatest for a sheath inlet width of 100 μm, which corresponded to the best sorting performance. The value of *R* increased by 57.9% when the width increased from 50 to 100 μm. This showed that the sorting performance was substantially improved. In summary, the optimal sheath fluid inlet width was 100 μm.

3.1.4 Influence of number of sheath liquid inlets on focusing and sorting of particles

The sheath flow could pinch the particles to improve the focusing performance. The number of sheath liquid inlets significantly impacted the sheath's pinch. To study the influence of the number of sheath liquid inlets, the position and width were set to $x_{in} = 890$ and 100 μm, respectively. The angle α was set to 90°. Figure 6 shows the focusing and sorting performances in the channel exit for different numbers of sheath fluid inlets.

The focusing performance dramatically improved when the number of sheath inlets was increased from one to two. The σ value of the 15-μm particles along the *y*-axis decreased by 31.9% when the number of sheath inlets was increased from one to two, which corresponded to a significant improvement of the focusing performance. However, the focusing performance underwent no evident change when the number of inlets was increased further. The particles could be focused best along the *y*-axis when the number of sheath inlets was six. The second-best focusing performances were achieved with two and four inlets for the 15- and 3-μm particles, respectively. This showed that multiple streams of the sheath liquid were significantly better than a single stream at the same total flow rate.

Good focusing of the channel particles did not mean that the structure was the best choice for particle sorting. The particle separation resolution of the channel structure with two sheath inlets was greater than those of the other channels, so particle sorting was favored when the number of sheath fluid inlets in the microchannel was two. The particle separation resolution increased by 55.2% when the number of sheath fluid inlets was increased from one to two. This was because the two inlets of sheath fluid created suitable Dean flow for sorting.

3.2 Force mechanism during particle focusing

The forces acting on the particles were explored using the channel device with the best focusing performance for each selection of parameter values. The relationship between the

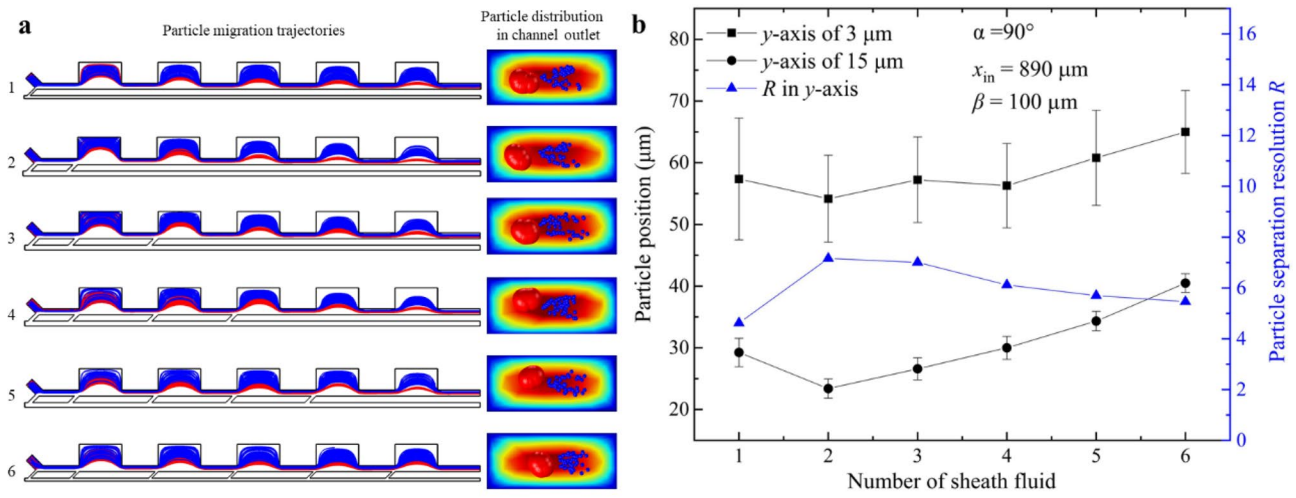

Fig. 6 Effects of the sheath inlet number: **a** particle migration trajectories (left) and particle distributions at the channel outlet (right), **b** focus positions of particles at the channel outlet

length of the channel and the forces on the particles was fitted. In this section, the angle α, sheath inlet position x_{in}, and sheath inlet width were set to 90°, 890 μm, and 100 μm, respectively.

3.2.1 Analysis of force characteristics of focused channel particles

Figure 7 shows the force changes of the 15-μm particles in the focusing channel in the *y*-direction along the length of the channel with six sheath liquid inlets. The sample flow had not yet intersected the sheath liquid flow at the

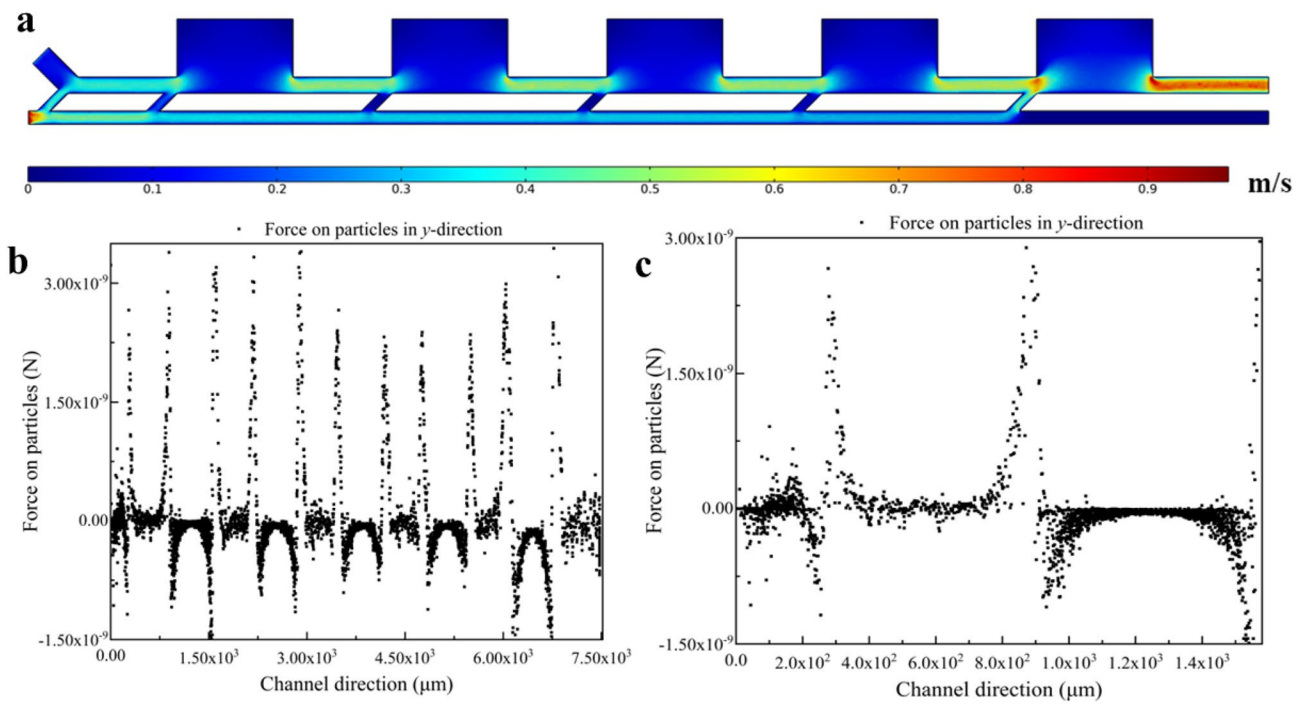

Fig. 7 **a** Cross-sectional flow field diagram, **b** distribution of particle forces in the *y*-direction, and **c** particle force distribution in first contraction–expansion area

channel entrance section ($x \le 0.28$ mm). As a result, the forces were relatively uniform for random particle distributions. In the first contraction area of the channel (0.28 mm $\le x \le$ 0.87 mm), as the particles continued to flow, the force distribution first decreased and then increased. The force was mainly in the positive *y*-direction, and thus, the particles moved in this direction. At the interface between the contraction area and the expansion area of the channel (0.87 mm $\le x \le$ 0.89 mm), the forces on the particles in the y-direction dropped linearly to the minimum value, which was a negative value. In the first expansion area of the channel (0.89 mm $\le x \le$ 1.58 mm), as the particles traveled further into the channel, the distribution of the forces in the *y*-direction along the *x*-axis first decreased and then increased. The forces were mainly negative, causing the particles to move in the negative *y*-direction. Similarly, the forces in the *y*-direction on the particles in the subsequent five contraction and expansion regions showed the same trends as that in the first area, and the analysis is not presented here. The forces at the interface area were caused by sheath flow and a Dean vortex, and the forces in other areas were inertial lift forces (Lee et al. 2009). The increase in the flow field's velocity at the channel's exit (6.0 mm $\le x \le$ 7.5 mm) led to increased forces acting on the particles in the *y*-direction at the exit. The overall trend was consistent with the first contraction zone.

3.2.2 Fitting of channel length and particle force focusing formula

To achieve the best focusing effect, the relationship between the forces on the particles in the *y*-direction and the length of the channel was determined by fitting. As shown in Fig. 7b, the forces on the particles in the *y*-direction exhibited a periodic change caused by the periodic flow channel structure. The forces on the particles in the *y*-direction changed significantly between contraction and expansion regions in the transition area.

The data from the third contraction–expansion area was selected for fitting, which was performed with the Origin software (Fig. 8a, b). The force differences between the contraction channel and the expansion channel were considered, and expressions relating the channel length and the forces on the particles in the *y*-direction were obtained by fitting.

Since the channel included five contraction–expansion regions, when the particle diameter (d_p) was 15 μm, the expression for the forces on the particles in the *y*-direction in the channel was a periodic function with a period (T) of 5:

$$F_y(x) = T\left[f_1(x) + f_2(x)\right](T = 5). \tag{1}$$

The forces acting on the particles needed to be greater than or equal to $F_y(x)$ to focus the particles in the channel. According to Newton's second law, in the *y*-direction,

$$F_y = \rho_p\left(\frac{\pi}{6}d_p^3\right)\frac{dV_y}{dt}. \tag{2}$$

Thus, T varied roughly linearly with the particle diameter cubed (d_p^3).

Therefore, the relationship between the shortest length (L_p) and the particle diameter required for particle focusing in the contracting and expanding flow channel with the introduction of multiple sheath fluid streams is deduced as follows:

$$\begin{aligned} L_p &= \frac{n\pi}{6}\frac{\rho_p d_p^3}{f(x_1)+f(x_2)}\frac{dV_y}{dt} \\ &\approx \frac{3}{2}n\left(n = \frac{5\times 15^3}{d_p^3}\right), \end{aligned} \tag{3}$$

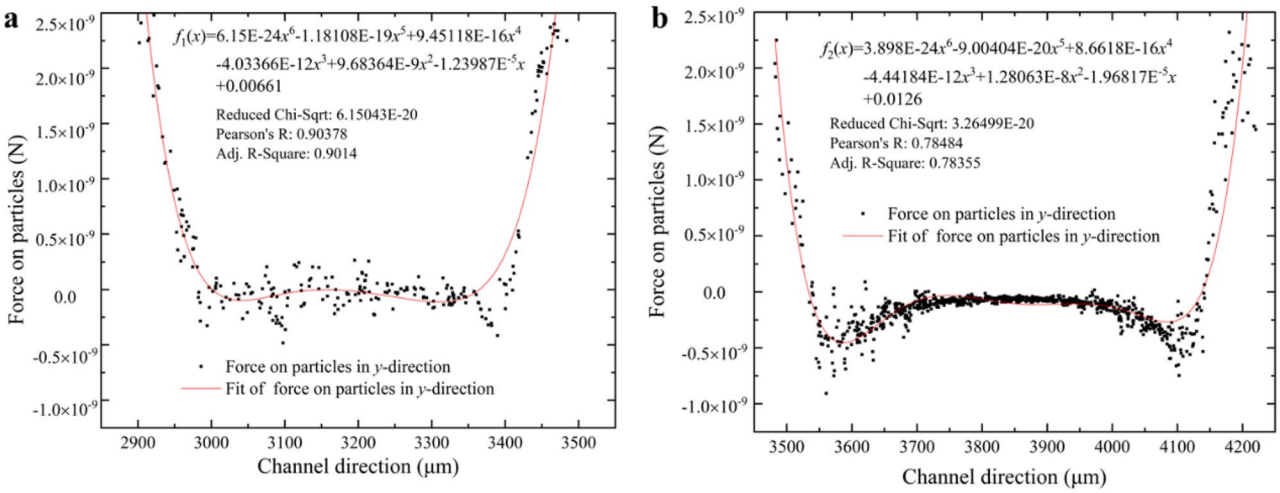

Fig. 8 Force distribution of particles in the *y*-direction: **a** force fitting in the contraction area, **b** force fitting in the expansion area

where n is the focal coefficient corresponding to particles of different diameters.

3.2.3 Verification of accuracy of fitting formula

The focusing of particles with diameters of 5 µm or greater can be achieved under the operating conditions described above. The critical requirements for realizing inertial focusing of particles with diameters of 5, 8, 10, and 20 µm were selected to verify the accuracy of the above fitting formula. According to the fitting formula, the shortest channel length required for complete focusing (period T rounded up to integer number) of particles with diameters of 5, 8, 10, and 20 µm were 202.5, 49.5, 25.5, and 4.5 mm, respectively.

As shown in Fig. 9 and Table 3, the required length of particle focusing derived from the fitting equation could entirely focus the above four types of particles. Therefore, the fitting relationship between the force of the particle and the length L_p required for particle focusing was reasonable.

Table 3 Particle distribution in the predicted channel outlet

Particle diameter (µm)	Predicted channel length (mm)	Particle standard deviation in the z-direction (µm)	Particle standard deviation in the y-direction (µm)
5	202.5	1.28	0.44
8	49.5	0.42	0.42
10	25.5	1.84	0.68
20	4.5	0.19	0.98

4 Conclusion

In this paper, a contraction–expansion array microchannel with multiple sheath fluids was proposed. This design increases the forces on the particles in the flow field. The dynamics of the particles in the microchannel were examined via simulation. The influence of the sheath fluid inlet angle, inlet position, inlet number, and inlet width on particle-focusing and sorting behavior were studied. At the same time, the forces on 15-µm particles and the minimum length required for focusing were analyzed. The conclusions were as follows:

(1) For the 0.095 and 0.475 m/s sheath fluid inlet velocities, the focusing and separation performances both greatly improved when the number of sheath fluid inlets increased from one to two due to the strengthening of the Dean vortex. The performances at these inlet velocities increased by 31.9% and 55.2%, respectively. When the inlet angle was 90°, the sheath fluid flow in the contraction–expansion design created an enormous flow vortex, and the particle focusing effect was the best due to suitable pinching of the sheath flow.

(2) Optimization of the sheath inlet width and position could effectively improve the focusing and sorting performances, and the improvement after optimizing each parameter exceeded 40%. For the 0.095 and 0.475 m/s sheath fluid inlet velocities, six sheath fluid inlets with widths of 100 µm and $x_{in} = 890$ µm were introduced to achieve the best focusing performance. The width of 100 µm created a suitable pinching effect of the sheath flow, and the sheath inflow in the expansion area enhanced the Dean flow.

(3) For particle sorting, the sorting effect increased first and then decreased with the increase in the number of sheath fluid inlets. When using two sheath fluid inlets, the

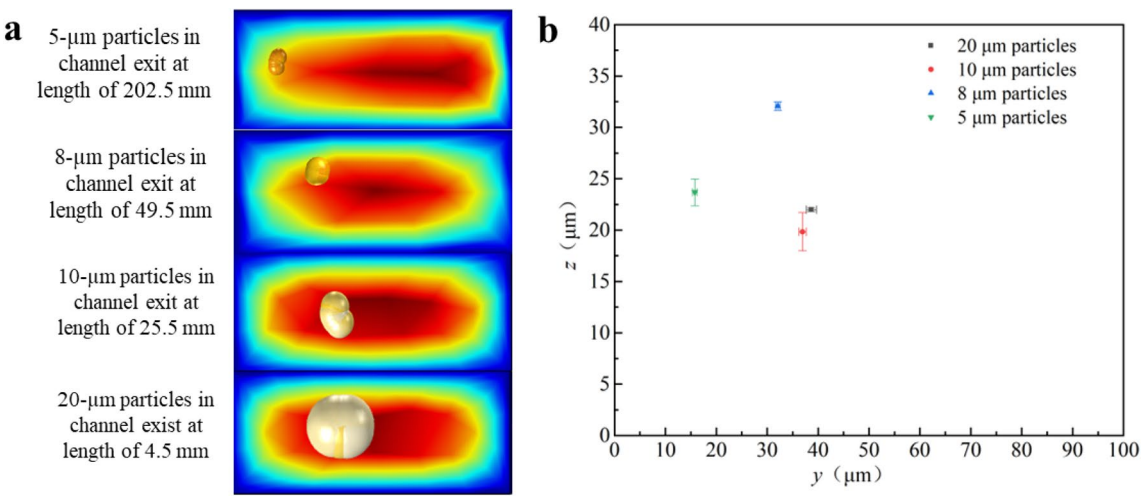

Fig. 9 **a** Particle distributions at predicted channel outlets for different particle sizes. **b** Particle focus positions at predicted channel outlets for different particle sizes

channel outlet was set at the center of the expansion area. The best sorting effect was achieved under this configuration due to the suitable Dean flow for sorting.

(4) The force mechanism of the particles in the contraction–expansion microchannels with multiple sheath fluid flows was analyzed, and expressions of the lateral forces of the particles were obtained. Based on the lateral force analysis, the correlation equation of the minimum length required for the particles to be entirely focused was fitted, and the accuracy of the correlation was verified.

Supplementary Information The online version contains supplementary material available at https://doi.org/10.1007/s10404-022-02620-5.

Acknowledgements This work was supported by the National Natural Science Foundation of China [grant numbers U20A20299, 51806038] and the Guangdong Special Support Program [grant number 2017TX04N371].

Author contributions Zhibin Wang: Methodology, Validation, Formal analysis, Investigation, Writing-review & editing.Tieshan Zhen: Conceptualization, Methodology, Formal analysis, Writing-original draft.Fan Wu: Methodology, Writing-review & editing.Songping Mo: Formal analysis, Writing-review & editing.Lisi Jia: Formal analysis, Validation.Ying Chen: Supervision.

Data Availability The data that support the findings of this study are available within the article and its supplementary material.

Declarations

Competing interests The authors declare no competing interests.

Conflict of interest The authors declare that they have no conflicts of interest.

References

Berger SA, Talbot L, Yao LS (1983) Flow in curved pipes. Annu Rev Fluid Mech 15(3):461–512. https://doi.org/10.1146/annurev.fl.15.010183.002333

Bhagat AAS, Kuntaegowdanahalli SS, Papautsky I (2008) Enhanced particle filtration in straight microchannels using shear-modulated inertial migration. Phys Fluids 20(101702):1–5. https://doi.org/10.1063/1.2998844

Carlo DD, Edd JF, Humphry KJ, Stone HA, Toner M (2009) Particle segregation and dynamics in confined flows. Phys Rev Lett 102(094503):1–4. https://doi.org/10.1103/PhysRevLett.102.094503

Choi S, Park JK (2008) Sheathless hydrophoretic particle focusing in a microchannel with exponentially increasing obstacle arrays. Anal Chem 80(8):3035–3039. https://doi.org/10.1021/ac8001319

De Rosa SC, Herzenberg LA, Herzenberg LA, Roederer M (2001) 11-color, 13-parameter flow cytometry: Identification of human naive T cells by phenotype, function, and T-cell receptor diversity. Nat Med 7(2):245–248. https://doi.org/10.1038/84701

Fan LL, Yu H, XuKun H, Liang Z, Jiang Z (2014) High-throughput, single-stream microparticle focusing using a microchannel with asymmetric sharp corners. Microfluid Nanofluid 17(68):639–646. https://doi.org/10.1007/s10404-014-1344-8

Fan LL, Yan Q, Zhe J (2018) Single particle train ordering in microchannel based on inertial and vortex effects. J Micromech Microeng 28(065011):1–10. https://doi.org/10.1088/1361-6439/aab57c

Gross HJ, Verwer B, Houck D, Recktenwald D (1993) Detection of rare cells at a frequency of one per million by flow cytometry. Cytometry 14(78):519–526. https://doi.org/10.1002/cyto.990140511

Hasegawa D, Bugarin C, Giordan M, Bresolin S, Longoni D, Micalizzi C, Ramenghi U, Bertaina A, Basso G, Locatelli F, Biondi A, Kronnie GT, Gaipa G (2013) Validation of flow cytometric phospho-STAT5 as a diagnostic tool for juvenile myelomonocytic leukemia. Blood Cancer J 3(160):1–6. https://doi.org/10.1038/bcj.2013.56

Huang D, Man J, Jiang D, Zhao J, Xiang N (2020) Inertial microfluidics: recent advances. Electrophoresis 41(14):2166–2187. https://doi.org/10.1002/elps.202000134

Hur SC, Tse HTK, Di Carlo D (2010) Sheathless inertial cell ordering for extreme throughput flow cytometry. Lab Chip 10(60):274–280. https://doi.org/10.1039/B919495A

Jiang D, Huang D, Zhao GT, Tang WL, Xiang N (2019) Numerical simulation of particle migration in different contraction–expansion ratio microchannels. Microfluid Nanofluid 23(1):7. https://doi.org/10.1007/s10404-018-2176-8

Jiang D, Ni C, Tang W, Huang D, Xiang N (2021) Inertial microfluidics in contraction-expansion microchannels: a review. Biomicrofluidics 15(41):1–19. https://doi.org/10.1063/5.0058732

Kalyan S, Torabi C, Khoo H, Sung HW, Choi SE, Wang W, Treutler B, Kim D, Hur SC (2021) Inertial microfluidics enabling clinical research. Micromachines 12(3):1–43. https://doi.org/10.3390/mi12030257

Lee MG, Choi S, Park JK (2009) Rapid laminating mixer using a contraction-expansion array microchannel. Appl Phys Lett 95(051902):1–3. https://doi.org/10.1063/1.3194137

Lee MG, Choi S, Park JK (2011) Inertial separation in a contraction–expansion array microchannel. J Chromatogr A 1218(28):4138–4143. https://doi.org/10.1016/j.chroma.2010.11.081

Lee MG, Shin JH, Choi S, Park JK (2014) Enhanced blood plasma separation by modulation of inertial lift force. Sens Actuators, B Chem 190(36):311–317. https://doi.org/10.1016/j.snb.2013.08.092

Li M, Muñoz HE, Schmidt A, Guo B, Lei C, Goda K, Di Carlo D (2016) Inertial focusing of ellipsoidal: euglena gracilis cells in a stepped microchannel. Lab Chip 16(20):4458–4465. https://doi.org/10.1039/C6LC01118G

Manz A, Graber N, Widmer HM (1990) Miniaturized total chemical analysis systems: a novel concept for chemical sensing. Sens Actuators B Chem 1(16):244–248. https://doi.org/10.1016/0925-4005(90)80209-I

Merkak O, Jossic L, Magnin A (2009) Migration and sedimentation of spherical particles in a yield stress fluid flowing in a horizontal cylindrical pipe. AIChE J 55(83):2515–2525. https://doi.org/10.1002/aic.11852

Raihan MK, Wu S, Dort H, Baghdady M, Song Y, Xuan X (2022) Effects of vertical confinement on the flow of polymer solutions in planar constriction microchannels. Soft Matter 18:7427–7440. https://doi.org/10.1039/D2SM01024K

Segre G, Silberg A (1961) Radial particle displacements in Poiseuille flow of suspensions. Nature 189(4760):209–210. https://doi.org/10.1038/189209a0

Seo KW, Choi YS, Lee SJ (2012) Dean-coupled inertial migration and transient focusing of particles in a curved microscale pipe flow. Exp Fluids 53:1867–1877. https://doi.org/10.1007/s00348-012-1403-4

Shahraki ZH, Navidbakhsh M, Taylor RA (2022) Coupling contraction-expansion arrays with spiral microchannels to enhance

microfluidic-based particle/cell separation. Int J Comput Fluid Dyn 36(1):63–90. https://doi.org/10.1080/10618562.2022.2053114

Soares R, Martins VC, Macedo R, Cardoso FA, Martins SAM, Caetano DM, Fonseca PH, Silvério V, Cardoso S, Freitas PP (2019) Go with the flow: advances and trends in magnetic flow cytometry. Anal Bioanal Chem 411(15):1839–1862. https://doi.org/10.1007/s00216-019-01593-9

Stavrakis S, Holzner G, Choo J, DeMello A (2019) High-throughput microfluidic imaging flow cytometry. Curr Opin Biotechnol 55(50):36–43. https://doi.org/10.1016/j.copbio.2018.08.002

Su HS, Wang ZB, Chen Y, Mo SP, An L (2020) Numerical simulation on interface dynamics of core coalescence of double-emulsion droplets. Ind Eng Chem Res 59:21248–21260. https://doi.org/10.1021/acs.iecr.0c04995

Sun DK, Xiang N, Chen K, Ni ZH (2013) Lattice Boltzmann modeling of particle inertial migration in a curved channel Wuli Xuebao. Acta Phys Sin 62(2):1–9. https://doi.org/10.7498/aps.62.024703

Tang WL, Xiang N, Zhang XJ, Huang D, Ni ZH (2015) Dynamic process and flow-rate regulation mechanism of particle inertial focusing in an asymmetric ally curved microchannel. Acta Phys Sin 64(18):184703

Tang W, Zhu S, Jiang D, Zhu L, Yang J, Xiang N (2020) Channel innovations for inertial microfluidics. Lab Chip 20(56):3485–3502. https://doi.org/10.1039/D0LC00714E

Wang ZB, Chen R, Zhu X, Liao Q, Ye DD, Zhang B, Jiao L (2018) Thermal analysis of the photothermal effect based droplet microfluidic system. Chem Eng Sci 186:191–198. https://doi.org/10.1016/j.ces.2018.04.049

Zhou Z, Chen Y, Zhu S, Liu L, Ni Z, Xiang N (2021) Inertial microfluidics for high-throughput cell analysis and detection: a review. The Analyst 146(20):6064–6083. https://doi.org/10.1039/D1AN00983D